Hindawi Publishing Corporation
Texture, Stress, and Microstructure
Volume 2009, Article ID 237485, 10 pages
doi:10.1155/2009/237485

Research Article

Using Individual Spectra Simulation for the Study of Pole Figures Errors

T. A. Lychagina,[1] D. I. Nikolayev,[1] and F. Wagner[2]

[1] *Frank Laboratory of Neutron Physics, Joint Institute for Nuclear Research, Dubna 141980, Moscow Reg., Russia*
[2] *Laboratoire d'Etudes des Textures et Application aux Matériaux (LETAM; CNRS FRE 3143), Ile du Saulcy, University Paul Verlaine-Metz, 57045 Metz, Cedex 01, France*

Correspondence should be addressed to T. A. Lychagina, lychagina@jinr.ru

Received 4 August 2008; Revised 20 November 2008; Accepted 26 March 2009

Recommended by Paul Houtte

Crystallographic texture is described by pole figures. In this paper, we continue to study experimental pole figure errors. In other words it can be named pole figure measurement errors. These errors are connected with the experimental procedure and do not depend on any further computations. In our previous works it was shown that the qualitative behaviour of pole figure measurement errors is similar to peak width determination errors. To check this conclusion a set of diffraction spectra were measured for Mg + 4.5%Al + 1%Zn sample on the spectrometer for quantitative texture analysis (SKAT) at FLNP, JINR, Dubna. Then we simulated the individual spectra and used these spectra for the pole figure extraction and the pole figure error determination. Such simulation enabled to confirm conclusions concerning the main role of the peak width determination error in the pole figure error. Additionally, we simulated individual spectra using model pole figures and extracted pole figures and pole figures errors from those spectra. For this case we also confirmed the same qualitative behaviour of pole figure measurement errors and peak width determination errors. The model pole figures were calculated on the basis of normal distributions.

1. Introduction

The neutron diffraction experiment is one of the methods for obtaining information about crystallographic texture. The spectrometer for quantitative texture analysis (SKAT) has been successfully operated at the 7A channel of IBR-2 reactor (FLNP, JINR, Dubna) since 1997 [1]. Measurements of spectra are provided using time-of-flight technique at pulsed reactor. The aim of texture neutron diffraction experiment is to determine the orientations of crystallites in a polycrystal. Neutron spectra are measured at SKAT to be used for pole figures extraction. We are interested in the integral intensity of individual peaks for the pole figure determination. 1368 spectra have to be processed simultaneously for complete pole figure. That corresponds to a 5-degree grid for the polar angle and azimuth as well (19×72).

Pole figures (PFs) contain experimental information about crystallographic texture. The requirements for the accuracy of PFs are growing in correlation with the complication of the investigated problems. Besides, it is necessary to take accurately the experimental errors into account for developing new instruments for quantitative texture analysis. Thus it is very important to study sources of the PF's measurement errors to look after their minimization. A set of papers [2–5] are devoted to this theme. In these works the main types of PF's measurement errors are analyzed. They are approximation errors connected to the instrument resolution and statistical errors connected to finite intensity of neutron sources and finite number of grains in measured textured samples. The study how counting statistics and exposure time influence the pole figure errors is described in [3], the influence of grain statistics is studied in [5] as well. It is necessary to underline that pole figures measurement errors have an integral character, that is, they include all factors like experimental layout, neutron statistics, grain statistics, external noise, and so forth. The local peak fit approach gives us a tool for pole figure intensity and pole figure measurement errors determination. This approach is described in our previous works [6, 7]. Pole figures measurement errors do not depend on ODF reconstruction methods

and are not connected with any further computations with pole figures, so they are of "pure" experimental kind. In our previous investigations [6, 7] it was established that the qualitative distribution of PF measurement errors is similar to the distribution of peak width determination errors. Thus, the errors of determination of the peak width play a determining role in the PF measurement errors. This statement is the starting point for the present work. To check this conclusion spectra simulations have been done. The purpose of such simulations is to be convinced that such behaviour of pole figure errors is a property not only of the spectrometer SKAT. It can be checked up by means of spectra simulations because the errors entered into the spectra at the simulations are not connected with a special measurement process.

2. Fundamentals

Denoting by dV volume of all crystallites in a sample which possesses an orientation g within orientation region dg, and by V the total sample volume, then the orientation distribution function (ODF) $f(g)$ is defined by [8]

$$\frac{1}{8\pi^2} f(g)dg = \frac{\mathrm{d}V(g)}{g}. \tag{1}$$

All rotations form the rotation group SO(3). The ODF is defined on the rotation group SO(3). As can be seen from definition the ODF is a normalized function:

$$\frac{1}{8\pi^2} \int_{\mathrm{SO}(3)} f(g)dg = 1. \tag{2}$$

Let $\vec{y}$ be the unit vector of a direction in the "sample coordinate system," $\vec{h}$ the unit vector of a direction described in the "crystal coordinate system" of a single crystal, then $\mathrm{d}V(\vec{h} \parallel \vec{y})$ is the volume fraction of the sample for which the crystallographic direction $\vec{h}$ coincides with $\vec{y}$ in $[\vec{y}, \vec{y} + \mathrm{d}\vec{y}]$. Thus, the pole figure $P_{\vec{h}_i}(\vec{y})$ is a function conformed to condition [8]:

$$\frac{1}{4\pi} P_{\vec{h}}(\vec{y})d\vec{y} = \frac{\mathrm{d}V\left(\vec{h} \| \vec{y}\right)}{V}. \tag{3}$$

The PFs are defined on the surface of a sphere S^2 with the normalization property [8]:

$$\frac{1}{4\pi} \int_{S^2} P_{\vec{h}}(\vec{y})d\vec{y} = 1. \tag{4}$$

The connection between the ODF and the PFs is given by the integral [9]:

$$P_{\vec{h}}(\vec{y}) = \frac{1}{2\pi} \int_0^{2\pi} f\left(\left\{\vec{h}, \varphi\right\}^{-1} \{\vec{y}, 0\}\right) d\varphi. \tag{5}$$

Equation (5) is the mathematical formulation of the main problem of quantitative texture analysis [10]. The notation $\{\vec{y}, 0\}$ means that a rotation g has corresponding Euler angles as two spherical ones of vector $\vec{y}$ and the third Euler angle is 0. (It is assumed that the first angle of rotation is about Z axis, the second one is about the new position of Y' and the last is about newer position of Z''.) Vector $\vec{h}$ can be considered as a properly rotated vector (001) and vector $\vec{y}$ could be considered as well as properly rotated vector (001). So the rotation g that connects vectors $\vec{h}$ and $\vec{y}$ could be expressed from the equation $\{\vec{h}, \tilde{\varphi}\}^{-1} \cdot (001) = g \cdot \{\vec{y}, \tilde{\tilde{\varphi}}\}^{-1} \cdot (001)$ or $g = \{\vec{h}, \tilde{\varphi} - \tilde{\tilde{\varphi}}\}^{-1} \cdot \{\vec{y}, 0\}$. Equation (5) utilizes the fact that pole figure describes the relative volume with $\vec{h} \,||\, \vec{y}$ and ODF describes the relative volume of grains having orientation g. So, to obtain the relative volume for which $\vec{h} \,||\, \vec{y}$ one needs to integrate ODF over φ, which is exactly expressed in (5).

The main problem of quantitative texture analysis is to reconstruct the ODF *f(g)* from a finite number of measured PFs $P_{\vec{h}_i}(\vec{y})$. In [9, 10] it was shown that this is an ill-posed problem because it has no unique solution. To overcome this problem several methods were developed [11–18]. The texture component method approximates the ODF by components of standard distributions [15–18]. In [19, 20] it was shown that (5) is the totally geodesic Radon transform on SO(3) and how this mathematical transform can be used in texture analysis.

In what follows for simulations we used circular normal distributions satisfying the central limit theorem on the rotation group SO(3) [18]. These distributions can also be obtained using approach of the Brownian motion on the rotation group SO(3) and sphere S^2 [21]. In case of axial texture the expressions for ODF components and PF components are given by the formulas [22]:

$$f^A(g, g_0, D, n_t) = \sum_{l=0}^{\infty} (2l+1)\exp(-l(l+1)D)P_l(\cos\beta), \tag{6}$$

$$P_{\vec{h}}^A(\vec{y}, \vec{n}_t) = \sum_{l=0(2)}^{\infty} (2l+1)\exp\{-l(l+1)D\}P_l(\cos\theta_1)P_l(\cos\theta_2), \tag{7}$$

where g_0 is the centre of the peak-like texture component, D is a width parameter connected with dispersion around the maximum of the texture component (or, e.g., with the half-width on a half maximum of the peak), $P_l(\cos\theta)$ are Legendre polynomials, $\vec{n}_t$ is the fibre axis, $\cos\beta = (g\vec{n}_t, g_o\vec{n}_t)$, $\cos\theta_1 = (\vec{h}, g_0\vec{n}_t)$, $\cos\theta_2 = (\vec{y}, \vec{n}_t)$. It is necessary to note that the described below results very likely would be quite similar if instead of the Brownian motion distributions (6), (7) one would use other type of a central distribution [23].

If the material has the crystal symmetry described by the point group $R_B = \{r_{B_i},\ i = 1, \ldots, M_B\}$ and a sample symmetry of the point group $R_A = \{r_{A_i},\ i = 1, \ldots, M_A\}$, where $G_B = \{g_{B_i},\ i = 1, \ldots, N_B\}$, $G_A = \{g_{A_i},\ i = 1, \ldots, N_A\}$

are their sub-groups of the rotation group SO(3) then the PFs and the ODFs are conformed to the symmetry conditions:

$$f(g) = f\left(g_{B_j} \cdot g \cdot g_{A_i}\right), \quad j = 1,\ldots,N_B,\ i = 1,\ldots,N_A;$$
$$P_h(\vec{y}) = P_{r_{B_j}h}(r_{A_i}\vec{y}), \quad j = 1,\ldots,M_B,\ i = 1,\ldots,M_A. \tag{8}$$

To satisfy symmetry conditions, (6), (7) should be rewritten in the form [10]:

$$f^S(g) = \frac{1}{N_A N_B}\sum_{i=1}^{N_A}\sum_{j=1}^{N_B} f\left(g, g_{B_j} g_0 g_{A_i}, D\right),$$

$$P_h^s(\vec{y}) = \frac{1}{M_A M_B}\frac{1}{2\pi}\sum_{i=1}^{M_A}\sum_{j=1}^{M_B}\int_0^{2\pi} f\left(\left\{r_{B_j}\vec{h},\varphi\right\}^{-1}\left\{r_{A_i}\vec{y},0\right\}\right)d\varphi$$

$$= \frac{1}{M_A M_B}\sum_{i=1}^{M_A}\sum_{j=1}^{M_B} P_{r_{B_j}\cdot h}(r_{A_i}\vec{y}). \tag{9}$$

In quantitative texture analysis is typical to estimate the quality of the an ODF reconstruction on the basis of recalculated pole figures $P_{h_i}^M(\vec{y}_j)$. In [24] "RP values" have been proposed that compare experimental and recalculated pole figures (recalculated using the ODF reconstructed by one of the methods):

$$RP_i = \frac{\sum_{j=1}^{J} RP_{i,j}(\varepsilon)}{\sum_{j=1}^{J}\Theta\left(\varepsilon, P_{\vec{h}_i}\left(\vec{y}_j\right)\right)}, \tag{10}$$

$$RP_{i,j}(\varepsilon) = 100[\%] * \frac{\left|P_{\vec{h}_i}\left(\vec{y}_j\right) - P_{\vec{h}_i}^M\left(\vec{y}_j\right)\right|}{P_{\vec{h}_i}\left(\vec{y}_j\right)}\Theta\left(\varepsilon, P_{\vec{h}_i}\left(\vec{y}_j\right)\right),$$
$$\Theta(\varepsilon, x) = \begin{cases} 0, & x < \varepsilon, \\ 1, & x \geq \varepsilon. \end{cases} \tag{11}$$

Here ε is a sensitivity level. The *RP* value is traditionally used as a quantitative characterization of the quality of an experimental pole figure. It characterizes the compatibility of the individual experimental PF values in order to be explained as a projection (5) of a three-dimensional distribution of *f(g)*. Since recalculated pole figures are computed using a ODF reconstructed from experimental data named "PFs" then such a PF error characterization obviously depends on the used ODF reconstruction method also. However it seems more natural to obtain information about pole figure measurement errors from the experimental data and to make attempts to have the obtained level of errors during ODF reconstruction and pole figures recalculation. In our previous papers [6, 7] we proposed a method to determine experimental pole figures measurement errors directly coming from the experiment and being independent on any ODF reconstruction methods. This approach is based on the determination of the main parameters of a diffraction peak by means of the analysis of the peak profile. To realize the proposed method for the PF measurement error determination new software was developed. It is worth to underline that these errors are not connected with any further computations.

The procedure used for peak processing can be called local peak fit in our case. We approximate each individual peak in contrast to the Rietveld texture analysis (RITA) concept widely used for neutron time-of-flight data treatment [25–27]. The RITA procedure is used, for example, to extract texture information from time-of-flight neutron spectra obtained by the diffractometer HIPPO (Los Alamos Neutron Science Centre) [27, 28]. In this case up to 240 spectra are simultaneously processed. The RITA concept was applied for processing data from the NSHR Dubna spectrometer too [29, 30]. In this case the spectrometer recorded 601 spectra, and in [29] only the half of the measured spectra (301) was used for processing including overlapped peaks and regions with heavy overlapping. In our case the local peak fit can be a reasonable procedure for data processing namely because of the huge number of data sets (1368 spectra).

It should be underlined that the local peak fit concept can be used for processing overlapped peaks typical for low crystal symmetries.

Texture measurements were carried out on the SKAT spectrometer for a set of Mg+4.5%Al+1%Zn samples. The PFs measurement errors were determined by the proposed method. It turned out that the qualitative behaviour of the pole figure measurement errors is similar to that of peak width parameter. To check this conclusion we simulated the individual spectra and used these spectra for the pole figure extraction and the pole figure measurement errors determination. Additionally, we simulated the individual spectra on the basis of model PFs.

3. Spectra Simulation

For our measurements the local part of the spectrum could successfully be approximated by a linear background and a bell-shaped function of the form [31]:

$$I(t) = \begin{cases} A_0 \exp\left(-\dfrac{(t-t_0)^2}{2\sigma_1^2}\right), & t \leq t_0, \\ A_0 \exp\left(-\dfrac{(t-t_0)^2}{2\sigma_2^2}\right), & t > t_0. \end{cases} \tag{12}$$

Here A_0 describes the peak amplitude, t_0 is for the peak position and σ_1, σ_2 describe the peak half-width from the left and right side of the peak maximum A_0, respectively. It is necessary to notice that the exact relationship between half-width at half maximum (HWHM) and the standard deviation of the normal distribution is the following: HWHM = $\sqrt{2\ln 2}\sigma \approx 1.178\sigma$. We consider the standard deviations σ_1, σ_2 as "peak half-width" from the left and right side of the peak maximum respectively. Such assumption will not influence on the main conclusions drawn on the basis of simulation. For shortness we name σ_1, σ_2 as peak half-width.

The input values for the spectra simulation were the experimental pole figure intensity $P_{\vec{h}_i}(\vec{y}_j)$, the peak position

t_0^i and the peak widths σ_1^i, σ_2^i where $i$the peaks numbers. The peak amplitude was obtained by the expression [6, 7]:

$$A_0^{ij} = \frac{2}{\sqrt{2\pi}} \frac{P_{\vec{h}_i}(y_j)}{\sigma_1^i + \sigma_2^i}. \tag{13}$$

The values for σ_1^i, σ_2^i were taken as the average over the half-width values $\sigma_{1j}^i, \sigma_{2j}^i$ determined from the $j = 1$, $N = 1368$ experimental spectra: $\sigma_1^i = (1/N)\sum_{j=1}^N \sigma_{1j}^i$, $\sigma_2^i = (1/N)\sum_{j=1}^N \sigma_{2j}^i$. So we can consider σ_1^i, σ_2^i as "unknown" input values.

Then our simulation was done in accordance to (12). The PFs are measured on the SKAT spectrometer using 19 detectors that register the neutron flux simultaneously for one sample position. Then the sample is rotated by 5-degree steps. $19 * 72 = 1368$ spectra are measured in total that corresponds to a 5 by 5 degree grid on the complete PF. That is why 1368 individual spectra were simulated for the Mg sample. Such a procedure was carried out for the several PFs that correspond to non-overlapped peaks. The background of the simulated spectra was approximated by the linear function:

$$Bkg = kt + b. \tag{14}$$

In Figure 1 a part of the simulated individual spectrum (a) as well as a part of the corresponding experimental individual spectrum (b) is presented. The intensity registered by this detector corresponds to the centre of the pole figures. This figure illustrates the quality of simulation. Then the simulation of spectra with errors (experimental "noise") was carried out. For that the following formula was used:

$$\widetilde{I}(t) = I(t)(1 + \tau\xi), \tag{15}$$

where ξ is a random value uniformly distributed in $[-1; 1]$, τ is a constant value from 0.01 up to 0.1. We used $\tau = 0.1$ for all simulated examples presented in this paper. Figure 2 shows the example of diffraction the $(10\bar{1}1)$ peak simulated (a) without experimental errors and (b) with simulated errors. Pole figure errors were also simulated in [32]. However, we simulate the errors (noise) directly in the spectra because actually the spectra contain the primary experimental information.

Then we repeated the afore-described procedure to simulate a set of spectra on the basis of model PFs. The model PFs were calculated using circular normal distributions. As far as our sample has an axial texture with the symmetry axis [001] we used (7) to simulate PFs. The simulated PFs are presented in Figure 7. They were derived for one texture component with $g_0 = \{0°, 0°, 0°\}$, $D = 0.0823$ and no random background (phon). The width parameter D corresponds to the real half width at half maximum HWHM $\approx 27.19°$ of the texture component. The HWHM-value for the Gaussian texture component with a normal distribution (6) was obtained numerically. Table 1 presents the connection between parameter D and HWHM of a normal texture component for some practical cases. The parameter l up to $L = 50$ was used to simulate pole figures

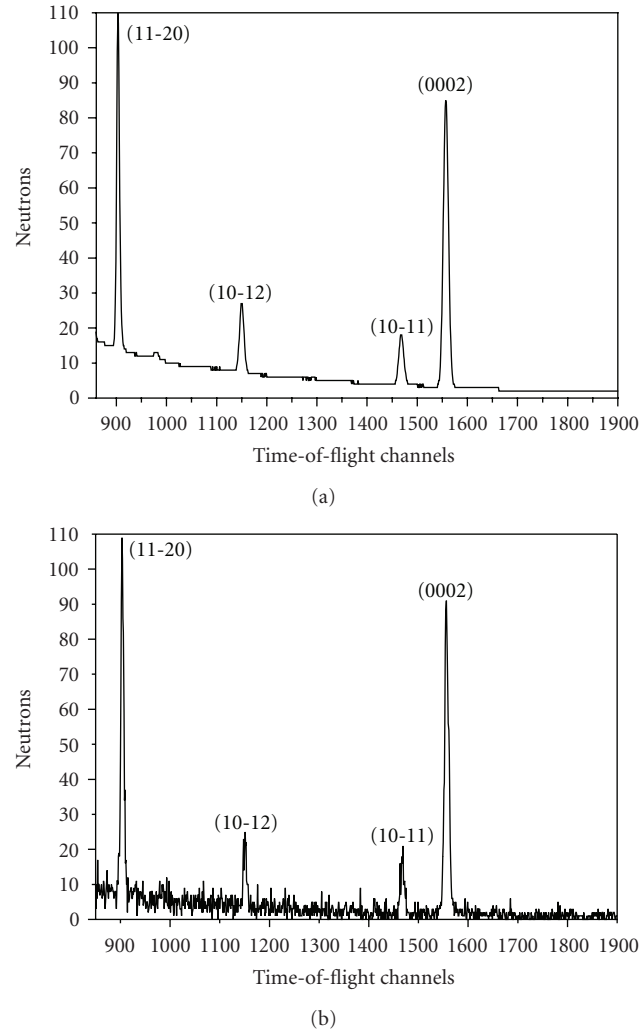

Figure 1: The dependence of the number of scattered neutrons on the number of channels of the time analyzer: (a) a part of the simulated individual spectrum, (b) a part of the corresponding experimental individual spectrum. The background is not subtracted. The channel width of the time analyzer is 64 μs. The number of reactor pulses during the measuring time for one individual spectrum was about 5700. It corresponds to ~19 min of measuring time for one individual spectrum.

according to (7). For the Mg sample we took hexagonal crystal symmetry into account in (7) supposing triclinic sample symmetry. It is needed to underline once more here that we consider only the pole figure measurement errors connected with the experimental procedure. That is why we do not investigate the influence of series truncation errors neglible for $L = 50$ in our case.

4. Results and Discussion

The simulated set of 1368 spectra for the Mg sample was processed using a spectra fit procedure described in what follows taking into account the peak shape given by (12). On the given part of the spectrum we found the best

Table 1: Connection between the parameter D and HWHM of a texture component (6) for some cases.

HWHM	0.5°	1°	3°	5°	10°	15°	20°	27.19°
D	3×10^{-5}	1×10^{-4}	9×10^{-4}	0.0027	0.0110	0.0248	0.0443	0.0823
HWHM	30°	40°	50°	60°	65°	70°	80°	90°
D	0.1005	0.1811	0.2879	0.4237	0.5034	0.5922	0.7983	1.0488

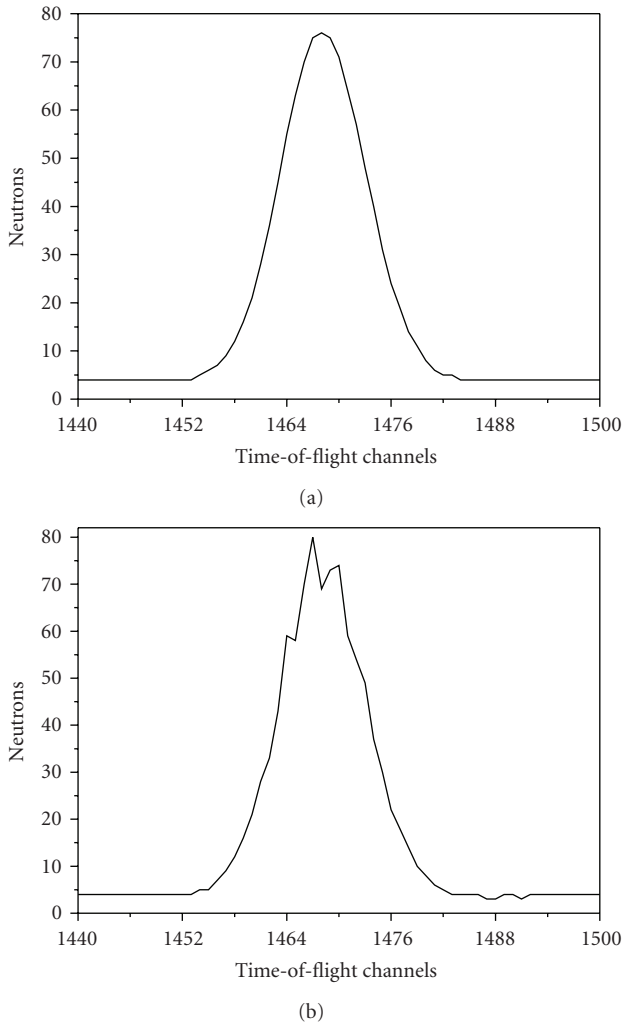

Figure 2: The dependence of the number of scattered neutrons on the number of channels of the time analyzer: (10-11) diffraction peak simulated (a) without experimental errors; (b) with errors, $\tau = 0.1$.

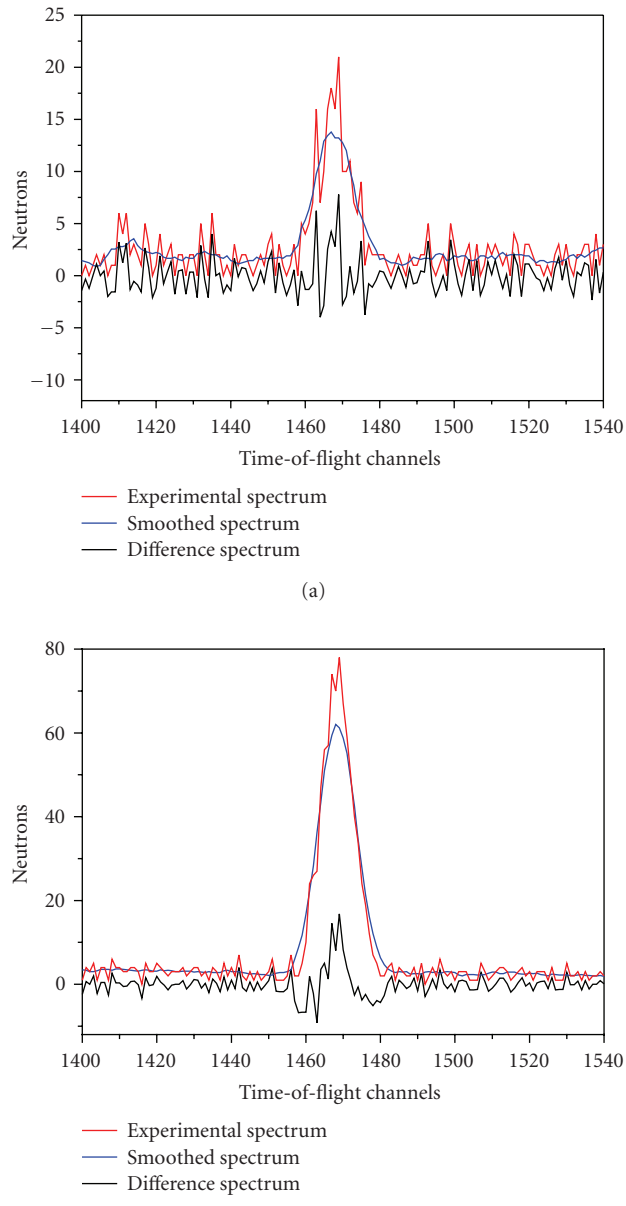

Figure 3: The dependence of the number of scattered neutrons on the channel number of the time analyzer. The picture illustrates the application of the Savitzky-Golay procedure for smoothing individual peaks with different signal-to-background ratios (by the example of the (10-11) peak): (a) smoothing of a poor reflection (signal-to-background ratio <10), (b) smoothing of a good reflection (signal-to-background ratio ~20). Original, smoothed and the difference spectra are shown.

approximation of the experimental data (intensity values in time-of-flight channels) by the calculated function which is the sum of the model peak components and linear background. We use the following approach for determining pole figure values and their errors in case of small peaks. If less than 16 points (y-coordinate of each point is counts of neutrons in a time channel) in a spectrum within the region of a specific peak not lying above background value,

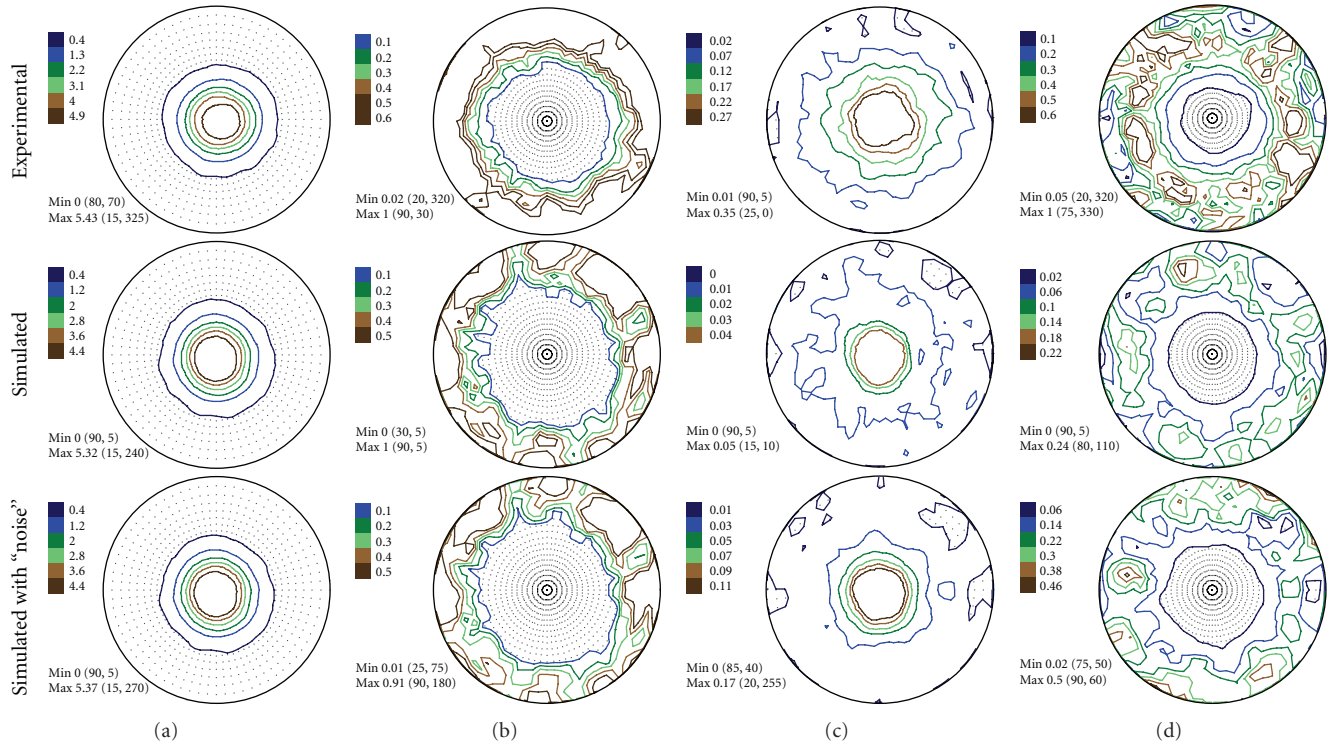

FIGURE 4: (a) Pole figures (0002). The intensities are given in mrd (multiples of random distribution). (b) The relative pole figure errors. (c) The errors of peak amplitude ΔA_0. (d) The errors of peak half-width $\Delta\sigma_1^2$.

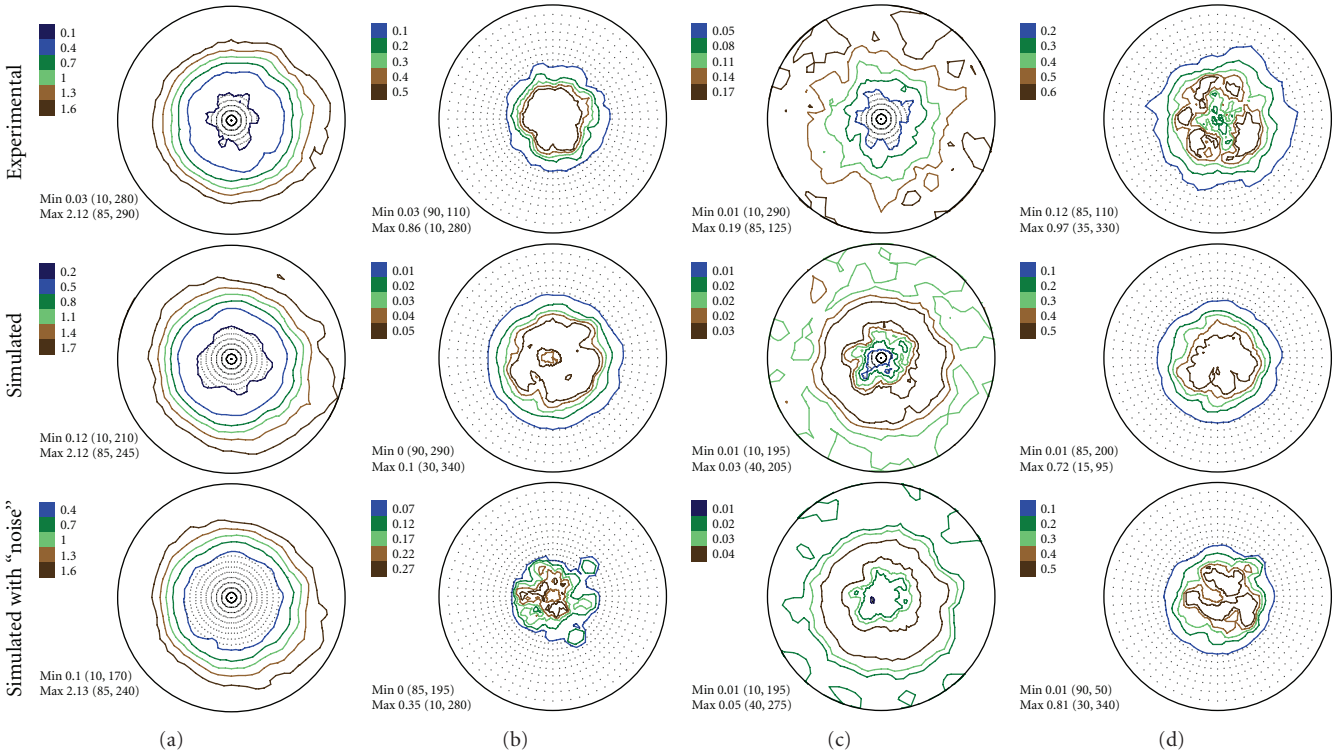

FIGURE 5: (a) Pole figures (10-10). The intensities are given in mrd (multiples of random distribution). (b) The relative pole figure errors. (c) The errors of peak amplitude ΔA_0. (d) The errors of peak half-width $\Delta\sigma_1^2$.

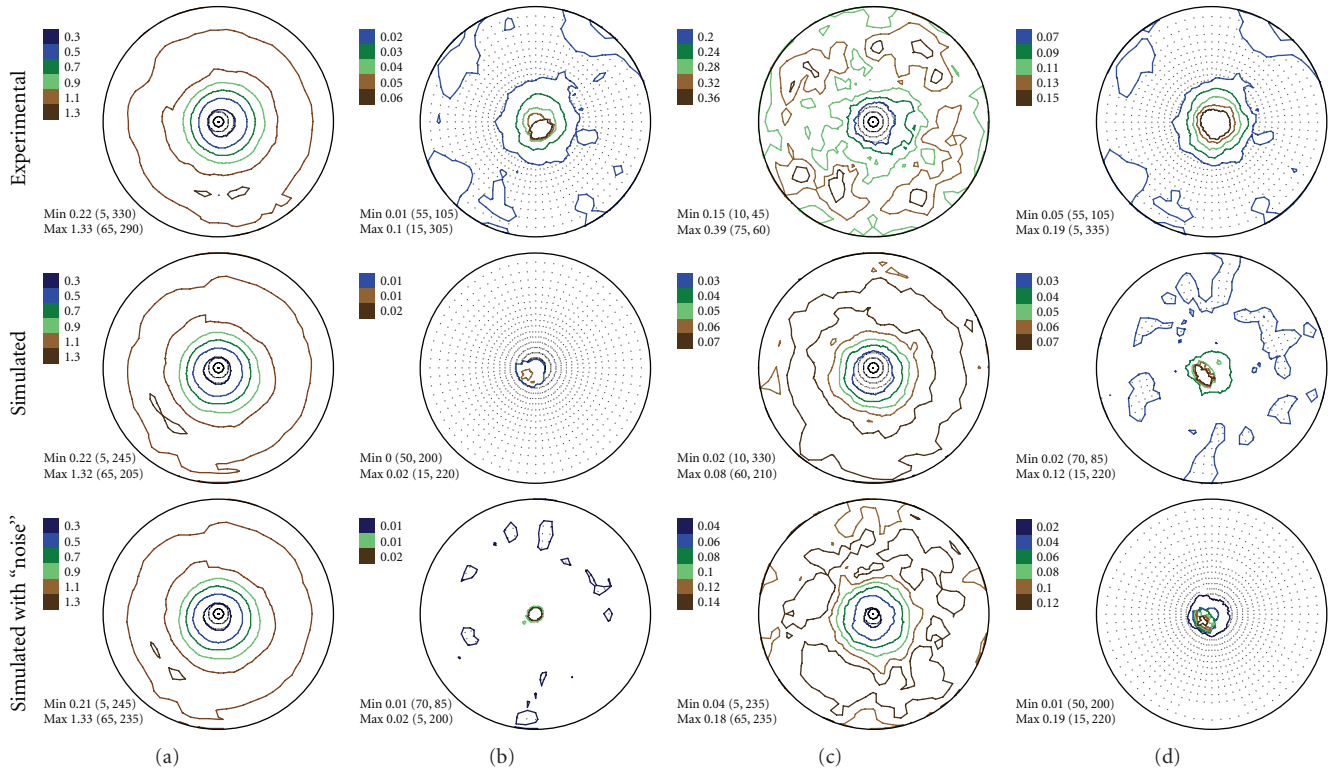

FIGURE 6: (a) Pole figures (10-11). The intensities are given in mrd (multiples of random distribution). (b) The relative pole figure errors. (c) The errors of peak amplitude ΔA_0. (d) The errors of peak half-width $\Delta\sigma_1^2$.

we assume that no peak is present and assign zero to pole intensity and 100% to a corresponding relative error. The typical (for a powder sample) number of points lying in the peak region above the background value is 30.

The fitting procedure was done by minimization of the module of the difference between the experimental data I and values of the approximating function $I(P)$ (12):

$$R = I - I(P), \tag{16}$$

where P is the set of fit parameters $(t_0, A_0, \sigma_1^2, \sigma_2^2)$ on which the minimization was carried out. The direct search complex algorithm [33, 34] was used for the minimization problem. The minimization routine applies the complex method to determine the minimum of a function of several variables. The method is based on function comparison; no smoothness is assumed. The errors of fitted parameters were determined in accordance with the generalized linear least squares method described in [35, Section 15.4, pages 665–667].

During the spectra processing for each of the $1368 = 19 * 72$ spectra and for each specific peak four parameters with uncertainties ΔA_0, Δt_0, $\Delta\sigma_1^2$, $\Delta\sigma_2^2$ were determined. So the pole figures themselves, the measurement errors of PFs and the peak half-width errors on the pole spheres were obtained. At this we used the formulas:

$$P_{h_i}\left(\vec{y}_j\right) = \frac{\sqrt{2\pi}}{2} A_0^{ij}\left(\sigma_1^{ij} + \sigma_2^{ij}\right), \tag{17}$$

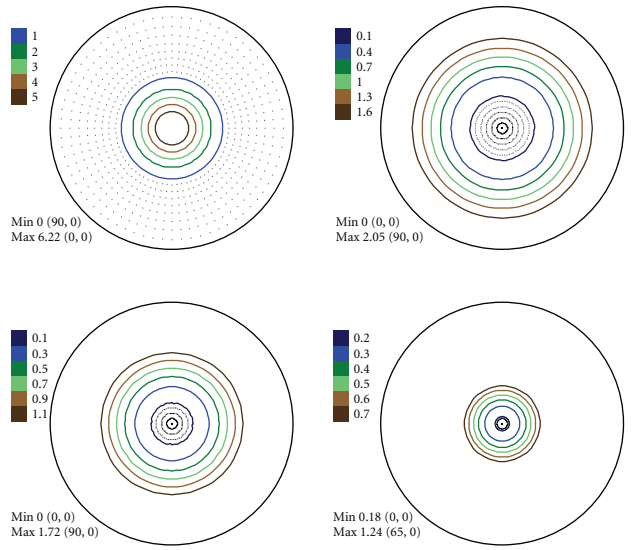

FIGURE 7: The model pole figures simulated by means of the circular normal distribution.

$$\frac{\Delta P_{h_i}\left(\vec{y}_j\right)}{P_{h_i}\left(\vec{y}_j\right)} = \frac{\sqrt{2\pi}}{2}\left(\frac{\Delta A_0^{ij}}{A_0^{ij}} + \frac{\left(\Delta\sigma_1^{ij} + \Delta\sigma_2^{ij}\right)}{\left(\sigma_1^{ij} + \sigma_2^{ij}\right)}\right). \tag{18}$$

The Pfs were obtained using a preliminary spectra smoothing, that is, the spectra were smoothed by the

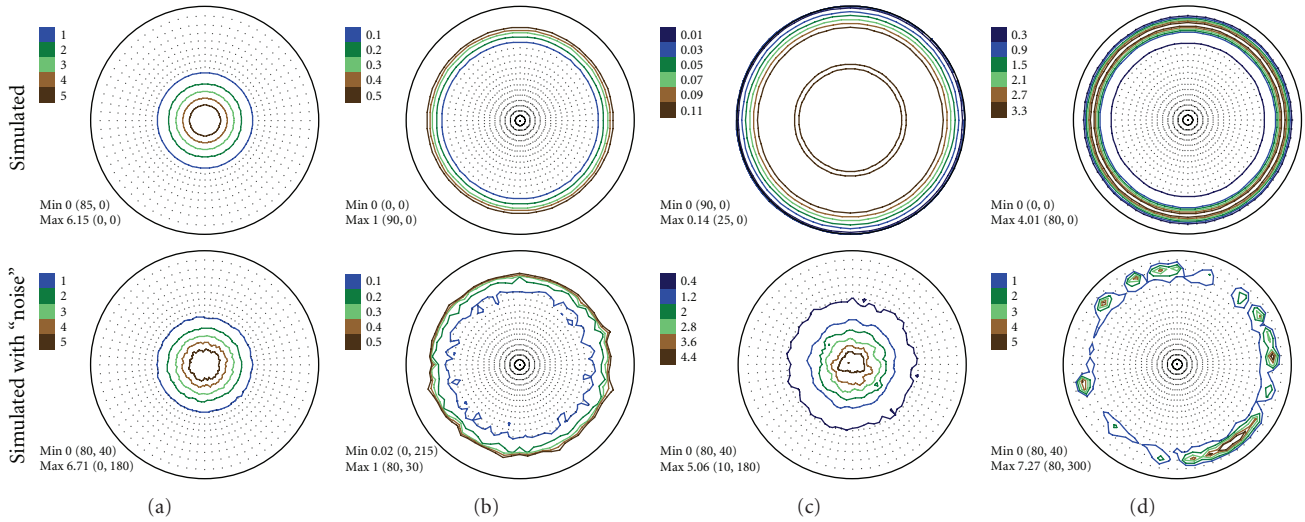

Figure 8: (a) The pole figures (0002) extracted from spectra simulated on the basis of the model PFs. The intensities are given in mrd (multiples of random distribution). (b) The relative pole figure errors. (c) The errors of peak amplitude ΔA_0. (d) The errors of peak half-width $\Delta\sigma_1^2$.

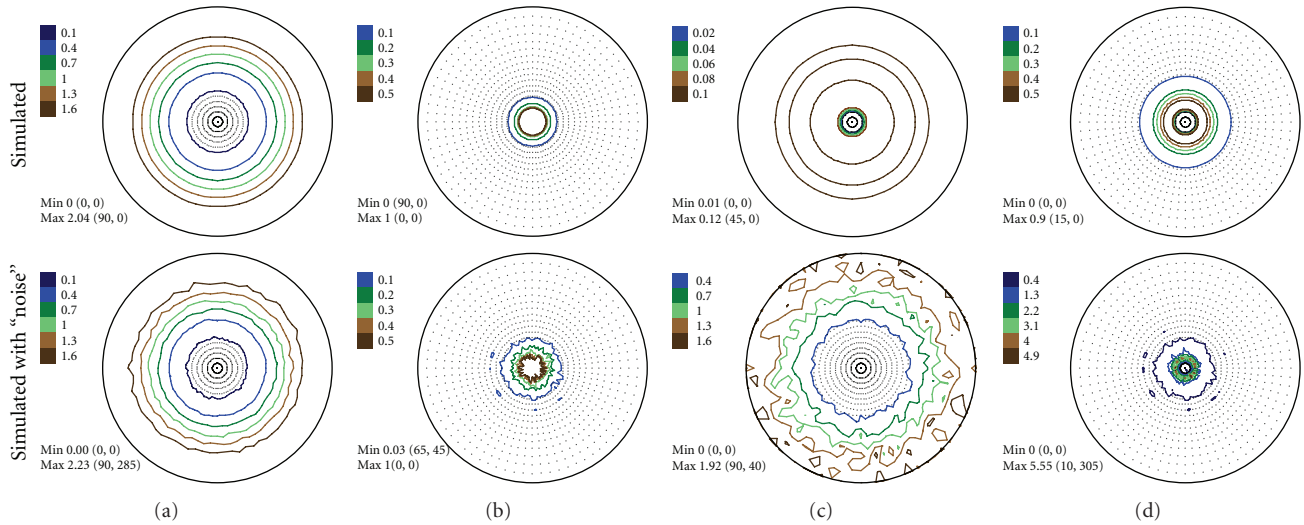

Figure 9: (a) The pole figures (10-10) extracted from spectra simulated on the basis of the model PFs. The intensities are given in mrd (multiples of random distribution). (b) The relative pole figure errors. (c) The errors of peak amplitude ΔA_0. (d) The errors of peak half-width $\Delta\sigma_1^2$.

Savitzky-Golay procedure [35] before the fit procedure described earlier . The smoothing was done by the specific moving average over six values. Details of the smoothing procedure are given in [35, Section 14.8]. Figure 3 illustrates the application of the smoothing procedure for a "good" and a "bad" peak. We consider a peak as a good one if the signal-to-background ratio is about or larger than 10.

In Figures 4–6 the experimental PFs are compared with those extracted from spectra simulated without and with simulated errors. The experimental pole figures errors were determined according to (18). The peak amplitude errors ΔA_0 and the peak half-width determination errors $\Delta\sigma_1^2$ are compared with those obtained from simulated spectra.

The experimental PFs presented in Figures 4(a)–6(a) were extracted from smoothed by the Savitzky-Golay procedure spectra. The presented pole figures and the errors have been smoothed according to the smoothing algorithm [36]. The smoothing of pole figures leads to an increase of the width-parameter D which describes the dispersion around the maximum of the normal distribution (7). Such smoothing allows paying more attention to the general behaviour of pole figures or functions on a sphere instead of fine details. It is appeared to be that the higher PF values the smaller error and on the contrary the smaller PF values the lager errors. This is in accordance with the knowledge of common spectrum analysis determining the

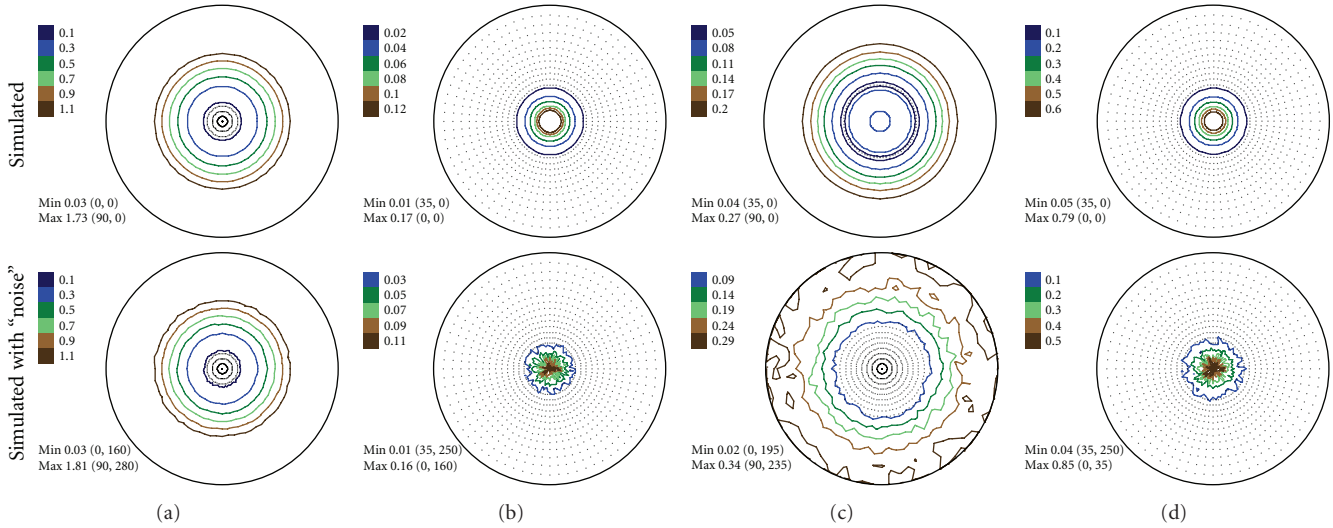

FIGURE 10: (a) The pole figures (10-11) extracted from spectra simulated on the basis of model PFs. The intensities are given in mrd (multiples of random distribution). (b) The relative pole figure errors. (c) The errors of peak amplitude ΔA_0. (d) The errors of peak half-width $\Delta\sigma_1^2$.

parameters of peak-like distribution [37]. One can see from Figures 4–6 that the qualitative distributions of pole figures errors are very similar to the distributions of peak half-width determination errors. The character of the peak amplitude error distributions is different from the distributions of pole figure errors. That is true for the experimental PFs and for PFs simulated without "noise" or with "noise" as well. Such results we obtained for the (0002), $(10\bar{1}0)$, $(10\bar{1}1)$ PFs. The statement is also confirmed by the spectra simulation carried out on the basis of simulated PFs (see Figures 8–10). So the conclusion about the main role of peak half-width determination error is drawn on the basis of the comparison of the errors distributions. At a first sight it seems that the conclusion concerning the dependence of the pole figure errors on the peak width errors directly follows from (17), (18) and in this case our conclusion is trivial and does not need experimental/empirical verification. However, (17), (18) are true only if (12) describing the peak form is adequate for our spectra. If a peak needs to be described using another form, then (17) and (18) are not necessary to be valid or vice versa. If after the treatment of our experimental and simulated spectra we were able to confirm our general conclusion then this is also a confirmation that the formula for the peak shape is appropriate.

5. Summary

The analysis of simulated spectra allowed us to confirm the main influence of the peak width determination error on the pole figure error. This conclusion is drawn on the basis of comparison of errors distributions. So we can state that a decrease of the pole figure errors can be reached by reducing of the peak width errors. One way to decrease the peak width error is to enlarge the peak width, but in this case the experimental resolution may be deteriorated. However, it can be done if the resolution in the diffraction spectrum is not so important (e.g., for texture investigations of samples with a sufficient number of isolated diffraction peaks). The deterioration of the resolution may increase the PF approximation error. However, in case of poorer collimation the statistical errors connected with the finite number of grains in a sample and with the finite number of counted neutrons will decrease. This will happen because the lower the collimation of the neutron beam the more intensity of scattered neutrons (neutron statistics) and the greater the number of grains in reflecting position (orientation statistics) we will get. So the question about the behaviour of the total PF error with deterioration of collimation is under consideration at present. Similar results can be expected for data collected with X-ray measurements using position sensitive detectors.

Acknowledgments

The present work is supported by INTAS Grant no. 03-51-6092 and RFBR (Russian Foundation for Basic Research) Grant no. 06-08-01193. The authors thank the anonymous referee, as well as Prof. S. Matthies and Prof. H. Schaeben for important remarks helping us to improve the manuscript.

References

[1] K. Ullemeyer, P. Spalthoff, J. Heinitz, N. N. Isakov, A. N. Nikitin, and K. Weber, "The SKat texture diffractometer at the pulsed reactor IBR-2 at Dubna: experimental layout and first measurements," *Nuclear Instruments and Methods in Physics Research A*, vol. 412, no. 1, pp. 80–88, 1998.

[2] A. Mücklich and P. Klimanek, "Experimental errors in quantitative texture analysis from diffraction pole figures," *Materials Science Forum*, vol. 157–162, pp. 275–286, 1994.

[3] V. V. Luzin and D. I. Nikolayev, "On the errors of the experimental pole figures," *Textures and Microstructures*, vol. 25, no. 2–4, pp. 121–128, 1996.

[4] V. V. Luzin and D. Nikolayev, "The errors of pole figures measured by neutrons," in *Proceedings of the 11th International Conference on Texture of Materials (ICOTOM 11)*, pp. 140–145, International Academic Publishers, Xi'an, China, September 1996.

[5] V. V. Luzin, "Optimization of texture measurements. IV. The influence of the grain-size distribution on the quality of texture measurements," *Textures and Microstructures*, vol. 31, no. 3, pp. 177–186, 1999.

[6] D. I. Nikolayev, T. A. Lychagina, A. V. Nikishin, and V. V. Yudin, "Study of error distribution in measured pole figures," *Solid State Phenomena*, vol. 105, pp. 77–82, 2005.

[7] D. I. Nikolayev, T. A. Lychagina, A. V. Nikishin, and V. V. Yudin, "Investigation of measured pole figures errors," *Materials Science Forum*, vol. 495–497, pp. 307–312, 2005.

[8] H. J. Bunge, *Texture Analysis in Material Science*, Butterworths, London , UK, 1982.

[9] S. Matthies, "On the reproducibility of the orientation distribution function of texture samples from pole figures (Ghost phenomena)," *Physica Status Solidi B*, vol. 92, no. 2, pp. K135–K138, 1979.

[10] S. R. Matthies, G. W. Vinel, and K. Helming, *Standard Distributions in Texture Analysis*, vol. 1, Akademie-Verlag, Berlin, Germany, 1987.

[11] M. Dahms and H. J. Bunge, "A positivity method for the determination of complete orientation distribution functions," *Textures and Microstructures*, vol. 10, no. 1, pp. 21–35, 1988.

[12] M. Dahms and H. J. Bunge, "The iterative series-expansion method for quantitative texture analysis. I. General outline," *Journal of Applied Crystallography*, vol. 22, no. 5, pp. 439–447, 1989.

[13] J. Imhof, "Texture analysis by iteration. II. Special cases of the general solution," *Physica Status Solidi B*, vol. 120, no. 1, pp. 321–328, 1983.

[14] S. Matthies and G. Vinel, "On the reproduction of the orientation distribution function of texturized samples from reduced pole figures using the conception of a conditional ghost correction," *Physica Status Solidi B*, vol. 112, no. 2, pp. K111–K114, 1982.

[15] K. Helming, *Texturapproximation durch Modellkomponenten*, Cuvillier, Göttingen, Germany, 1996.

[16] T. Eschner, *Quantitative Texturanalyse durch Komponentenzerlegung von Beugungs-Polfiguren*, dissertation, TU Bergakademie Freiberg, Göttingen, Germany, 1994.

[17] T. Eschner, "Generalized model function for quantitative texture analysis," in *Textures of Geological Materials, Proceedings of a Workshop, DGM Informationsgesellschaft*, H. J. Bunge, S. Siegesmund, W. Skrotzki, and K. Weber, Eds., pp. 15–28, Oberursel, Germany, 1994.

[18] T. I. Savyolova, "Distribution function of grains with respect to polycrystal orientations and its. Gaussian approximation," *Zavodskaya Laboratoriya*, vol. 50, no. 4, pp. 48–52, 1984 (Russian).

[19] K. G. van den Boogaart, R. Hielscher, J. Prestin, and H. Schaeben, "Kernel-based methods for inversion of the Radon transform on SO(3) and their applications to texture analysis," *Journal of Computational and Applied Mathematics*, vol. 199, no. 1, pp. 122–140, 2007.

[20] R. Hielscher, *The radon transform on the rotation group—inversion and application to texture analysis*, Ph.D. thesis, TU Bergakademie Freiberg, Göttingen, Germany, 2007.

[21] P. H. Roberts and D. E. Winch, "On random rotation," *Advances in Applied Probability*, vol. 16, no. 12, pp. 638–655, 1984.

[22] T. I. Bucharova, *Izvestiya, Physics of the Solid Earth*, vol. 6, pp. 59–67, 1993 (Russian).

[23] H. Schaeben and D. I. Nikolayev, "The central limit theorem in texture component fit methods," *Acta Applicandae Mathematicae*, vol. 53, no. 1, pp. 59–87, 1998.

[24] S. Matthies, H. R. Wenk, and G. Vinel, "Some basic concepts of texture analysis and comparison of three methods to calculate orientation distributions from pole figures," *Journal of Applied Crystallography*, vol. 21, no. 4, pp. 285–304, 1988.

[25] L. Lutterotti, S. Matthies, H.-R. Wenk, A. S. Schultz, and J. W. Richardson Jr., "Combined texture and structure analysis of deformed limestone from time-of-flight neutron diffraction spectra," *Journal of Applied Physics*, vol. 81, no. 2, pp. 594–600, 1997.

[26] R. B. Von Dreele, "Quantitative texture analysis by Rietveld refinement," *Journal of Applied Crystallography*, vol. 30, no. 4, pp. 517–525, 1997.

[27] S. Vogel, C. Hartig, L. Lutteroti, R. B. Von Dreele, H.-R. Wenk, and D. J. Williams, "Texture measurements using the new neutron diffractometer HIPPO and their analysis using the rietveld method," *Advance in X-Ray Analysis*, vol. 47, pp. 431–436, 2004.

[28] S. Matthies, J. Pehl, H.-R. Wenk, L. Lutterotti, and S. C. Vogel, "Quantitative texture analysis with the HIPPO neutron TOF diffractometer," *Journal of Applied Crystallography*, vol. 38, no. 3, pp. 462–475, 2005.

[29] S. Matthies, L. Lutterotti, K. Ullemeyer, and H. R. Wenk, "Texture analysis of quartzite by whole pattern deconvolution," *Textures and Microstructures*, vol. 33, no. 1–4, pp. 139–149, 1999.

[30] K. Walther, J. Heinitz, K. Ullemeyer, M. Betzl, and H.-R. Wenk, "Time-of-flight texture analysis of limestone standard: dubna results," *Journal of Applied Crystallography*, vol. 28, no. 5, pp. 503–507, 1995.

[31] C. G. Windsor, *Pulsed Neutron Scattering*, Taylor and Francis, London, UK, 1981.

[32] J. V. Bernier, M. P. Miller, and D. E. Boyce, "A novel optimization-based pole-figure inversion method: comparison with WIMV and maximum entropy methods," *Journal of Applied Crystallography*, vol. 39, no. 5, pp. 697–713, 2006.

[33] E. Gill Philip, W. Murray, and M. Wright, *Practical Optimization*, Academic Press, New York, NY, USA, 1981.

[34] J. A. Nelder and R. Mead, "A simplex method for function minimization," *Computer Journal*, vol. 7, no. 4, pp. 308–313, 1965.

[35] W. H. Press, S. A. Teukolsky, W. T. Vetterling, and B. P. Flannery, *Numerical Recipes in FORTRAN. The art of Scientific Computing*, Cambridge University Press, Cambridge, UK, 2nd edition, 1992.

[36] D. Nikolayev and K. Ullemeyer, "Note on preprocessing of diffraction pole-density data," *Journal of Applied Crystallography*, vol. 27, no. 4, pp. 517–520, 1994.

[37] G. V. Vinel and S. Matthies, *Communication of Zfk (Zenralinstitut fur Kernforschung Rossendorf bei Dresden)*, no. 391, 1979, Akademie der Wissenschaften der DDR.